Properties of backscattered ultraviolet reflectances in cloudy atmosphere

Z. Ahmad
Science and Data Systems, Inc., Silver Spring, Maryland

P. K. Bhartia
NASA Goddard Space Flight Center, Greenbelt, Maryland

N. Krotkov
Goddard Earth Sciences and Technology Center,
University of Maryland Baltimore County, Baltimore, Maryland

Popular Summary

We use a Plane-Parallel Cloud (PPC) model to illustrate how Mie scattering from cloud particles interacts with Rayleigh scattering in the atmosphere and produces a complex wavelength dependence in the top-of-the-atmosphere (TOA) reflectances measured by satellite instruments that operate in the ultraviolet (UV) part of the spectrum. Comparisons of the PPC model-derived spectral dependence of reflectances with the Total Ozone Mapping Spectrometer (TOMS) measurements show surprisingly good agreement over a wide range of observational conditions. The PPC model results also are compared with the results of two other cloud models: Lambert Equivalent Reflectivity (LER) and Modified Lambert Equivalent Reflectivity (MLER) that have been used to analyze satellite data in the UV. These models assume that clouds are opaque Lambertian reflectors rather than Mie scattering particles. Although one of these models (MLER) agrees reasonably well with the data, the results from this model appear somewhat unphysical and may not be suitable for interpreting satellite data if one desires high accuracy. We also use the PPC model to illustrate how clouds can perturb tropospheric O_3 absorption in complex ways that cannot be explained by models that treat them as reflecting surfaces rather than as volume scatterers.

Properties of backscattered ultraviolet reflectances in cloudy atmosphere

Z. Ahmad

Science and Data Systems, Inc., Silver Spring, Maryland

P. K. Bhartia

NASA Goddard Space Flight Center, Greenbelt, Maryland

N. Krotkov

Goddard Earth Sciences and Technology Center,

University of Maryland Baltimore County, Baltimore, Maryland

Abstract

We use a Plane-Parallel Cloud (PPC) model to illustrate how Mie scattering from cloud particles interacts with Rayleigh scattering in the atmosphere and produces a complex wavelength dependence in the top-of-the-atmosphere (TOA) reflectances measured by satellite instruments that operate in the ultraviolet (UV) part of the spectrum. Comparisons of the PPC model-derived spectral dependence of reflectances with the Total Ozone Mapping Spectrometer (TOMS) measurements show surprisingly good agreement over a wide range of observational conditions. The PPC model results also are compared with the results of two other cloud models: Lambert Equivalent Reflectivity (LER) and Modified Lambert Equivalent Reflectivity (MLER) that have been used to analyze satellite data in the UV. These models assume that clouds are opaque Lambertian reflectors rather than Mie scattering particles. Although one of these models (MLER) agrees reasonably well with the data, the results from this model appear somewhat unphysical and may not be suitable for interpreting satellite data if one desires high accuracy. We also use the PPC model to illustrate how clouds can perturb tropospheric O_3 absorption in complex ways that cannot be explained by models that treat them as reflecting surfaces rather than as volume scatterers.

1.0 Introduction

In the past 30 years, a number of satellite instruments, including Total Ozone Mapping Spectrometer (TOMS), Solar Backscattered Ultraviolet (SBUV), and Global Ozone Mapping Experiment (GOME), and most recently, SCanning Imaging Absorption SpectroMeter for Atmospheric CHartographY (SCIAMACHY) have been launched to measure the backscattered solar radiation at high-spectral resolution to derive ozone and other trace gases in the atmosphere (see, for example, Mateer et al., 1971; Klenk et al., 1982; Bhartia et al., 1996; Chance, 1998; Thomas et al., 1998; Burrows et al., 1999; Bovensmann et al.; 1999, and Chance et al., 2000). Because the field-of-view of these instruments is ~100 km, clouds are almost always present and they must be accounted for in retrieving the trace gases.

In this paper, we focus on the spectral properties of backscattered ultraviolet (buv) reflectances in cloudy atmosphere. Visible measurements of radiation fields above the clouds show that the reflection from the clouds is highly anisotropic and depends on the angle of illumination (Salomonson, 1968). Although the cloud scattering, by itself, has no spectral dependence between visible and ultraviolet (UV), the strong wavelength-dependent molecular scattering in UV adds significant complications to analyzing the buv data.

We use a one-dimensional Plane-Parallel Cloud (PPC) model to examine how clouds modify the spectral dependence of the emerging radiation at the top of the atmosphere. We then compare these findings with the spectral dependence observed by

the TOMS instrument that flew on the Nimbus-7 satellite for more than 13 years. We also examine the results of two simple cloud models: Lambert Equivalent Reflectivity (LER) and Modified Lambert Equivalent Reflectivity (MLER). A number of investigators have proposed these two cloud models to explain the spectral dependence of buv reflectances (*see for example*, Eck et al., 1995; McPeters et al., 1996; Hsu et al., 1997; Koelemeijer and Stammes 1999; Koelemeijer and Stammes, 2000; and Krotkov et al., 2001). We find that the PPC model agrees surprisingly well with the observations over a wide range of observing conditions without the need of any "tuning" parameters as required by the other models. Finally, using the PPC model, we also show how the absorption of buv radiances by the tropospheric ozone is altered by multiple scattering within and outside the cloud and by multiple reflections between the cloud and the snow on the ground.

2.0 Radiative Transfer (RT) Model

In most RT simulations, the cloud-droplet size distribution often is described by some form of a modified gamma distribution (Deirmendjian, 1963, 1964, and 1969). Hansen (1971) used such a distribution to describe fair-weather cumulus clouds. King and Harshvardhan (1986) used this distribution to compare the cloud albedo, transmission, and absorption calculated by different RT programs. Rossow and Schiffer (1999) have made the same assumption to retrieve cloud optical properties from the satellite measurements for the International Satellite Cloud Climatology Project (ISCCP).

For this study, we use Deirmendjian's C1 distribution with an effective radius of 6 μm and a maximum radius of 15 μm to describe the cloud-droplet size distribution. Although, in the strictest sense, this model is valid only for cumulus clouds of moderate optical thickness (Deirmendjian, 1969), the spectral dependence of buv reflectances, the primary issue in this paper, is largely insensitive to the assumed cloud size distribution and effective radius. We assume spherical cloud droplets with a $1.340 - 0.0i$ refractive index, independent of wavelength. Scattering phase function calculated using the Mie theory gives an asymmetry factor, g of 0.859 at 380 nm. For the purposes of the RT simulations, we also assume the clouds are uniform vertically and infinite horizontally. We carry out simulations for mid-level and low-level cloud scenarios. For mid-level scenarios, the cloud top is placed at 500 hPa and the bottom at 700 hPa. For low-level scenarios, the cloud top is placed at 700 hPa and the bottom at 850 hPa. We also carry out a few special simulations with the cloud top at 200 hPa and the bottom at 800 hPa to represent deep-convective clouds. There are no aerosols in the model atmosphere. For

the lower boundary, we assume a Lambertian surface at 1013 hPa to represent various terrestrial and ocean surfaces.

Most of the analyses presented in this paper are for a 340- and 380-nm wavelength, where the Rayleigh optical depths are 0.712 and 0.446, respectively. Although there is some ozone absorption at 340 nm, we assume it to be zero in our simulations. For comparison with satellite data, the observed radiances are corrected for the ozone absorption using the ozone amount derived from the satellite data. Also, a few simulations for 317.5 nm are carried out to study the effect of clouds on tropospheric ozone absorption. In these simulations, a standard mid-latitude ozone profile containing 325 DU of total ozone is used.

For optical thickness of clouds up to 20, we use a modified version of the Herman and Browning code (1965) called MODified RADtran (MODRAD) (Ahmad and Fraser, 1982) to simulate the upwelling radiance at the top of the atmosphere. This code divides the atmosphere into plane-parallel layers and performs numerical integration over the optical thickness, the polar angle, and the azimuth angle. MODRAD uses the Gauss Seidel iterative method to solve the RT equation for the model atmosphere. The MODRAD code is a vector code that accounts for all orders of scattering and polarization. We apply a first-order pseudo-sphericity correction in which the solar beam is attenuated by considering sphericity, but the scattering is considered in a plane-parallel atmosphere. For optical thickness of clouds greater than 20, we use the DIScrete ORdinaTe (DISORT) code (Stamnes et al., 1988). It is a much faster code than

MODRAD, particularly for optically thick clouds, but because it is a scalar code, it is less reliable in the UV wavelengths when cloud optical thickness is small. For cloud optical thickness of 20, the agreement between MODRAD and DISORT is better than ~1%.

3.0 Cloud Reflectance in the Ultraviolet (UV)

Because clouds consist of large particles, they alone are not expected to show any wavelength dependence in their reflective or transmitting properties. However, because of large asymmetry factors and optical density (optical thickness), clouds show strong angular anisotropy in their reflective properties. In this section, we first show the Bi-directional Reflectance Distribution Function (BRDF) of clouds (which is calculated in the absence of molecular atmosphere). We then compare it with the top-of-the-atmosphere (TOA) reflectances, defined as $\rho(\mu,\varphi, \mu_o,\varphi_o) = \pi I(\mu,\varphi, \mu_o,\varphi_o)/ \mu_o F$, where $I(\mu,\varphi, \mu_o,\varphi_o)$ is the upwelling radiance and F is the extra-terrestrial solar irradiance. The following symbols: μ_o and μ, respectively, are the cosine of the solar zenith angle (θ_0) and the view angle (θ). The symbols φ_o and φ, respectively, are the solar azimuth and view azimuth angles. As will be seen, the TOA reflectances are strongly affected by molecular scattering in the UV and show strong wavelength dependence.

3.1 Angular Dependence

Figure 1(a) shows the nadir reflectance of clouds in the absence of any molecular or particulate atmosphere. One finds that for low-surface albedo, the reflectance increases with cloud optical thickness (τ_{cloud}) and that the rate of increase (in the reflectance value) is larger at small τ_{cloud} than at large τ_{cloud}. The nadir reflectance decreases with an increase in solar zenith angle (which is not always the case for off-

nadir observations). These features can be easily understood if one recognizes the fact that for small values of τ_{cloud}, the scattering is proportional to the phase function and the number of particles in a cloud column, whereas at large values of τ_{cloud}, the multiple-scattering contribution becomes large and the emerging radiation becomes more isotropic. Also, as solar zenith angle (θ_0) increases, the effective scattering layer in the cloud moves upward. At very large values of θ_0, it is near the top of the cloud where more photons escape the surface in the near-forward direction than in the direction normal to the surface (the nadir direction). This fact explains why, for example, for τ=20, the reflectance value is 0.7 for overhead sun and 0.53 for θ_0=78°.

The angular anisotropy in the cloud reflectance is better seen in the polar plot shown in Figure 1(b). The graph is for θ_0=62° and is normalized with respect to the reflectance value in the nadir direction (θ=0°). It shows strong anisotropy in the principal plane and very weak anisotropy in a plane perpendicular to it. For example, in the forward direction (φ=0°), the reflectance value at θ=60° is three times the value in the nadir direction, whereas at the same view angle in the backward direction (φ=180°), it is slightly greater than two times the value in the nadir direction. On the other hand, the anisotropy is weakest in a plane perpendicular to the principal plane. This difference can be seen from the reflectance value, which is about 1.4 times the nadir value at the same view angle of θ=60°. It should be noted here that most Total Ozone Mapping Spectrometer (TOMS) measurements are in the plane perpendicular to the principal plane. Also, because of distortion of the field-of-view due to Earth's sphericity, TOMS and most satellite instruments do not measure reflectances at viewing angles greater than

63°. (Strictly speaking, this angle depends on the satellite view angle and the altitude of the satellite.)

We stated earlier that the Rayleigh scattering modifies the BRDF of clouds. Figure 2(a) shows the ratio of the TOA nadir reflectance with molecular atmosphere to the nadir reflectance without molecular atmosphere ($\rho^{atm}/\rho^{no\text{-}atm}$) is plotted against the optical thickness of the cloud (τ_{cloud}). Figure 1(a) shows that for small values of τ_{cloud}, the Rayleigh scattering contribution from the molecular atmosphere is much larger than the Mie scattering contribution from the cloud. Figure 1 also shows that the ratio strongly depends on the solar zenith angle (θ_0) of the incident radiation. The ratio is about 3.5 for overhead sun and about 5.8 for a solar zenith angle of 78°. However, with an increase in τ_{cloud}, the Mie scattering contribution from the cloud overwhelms the Rayleigh scattering from the molecular atmosphere. One finds that the ratio is practically 1 for τ_{cloud} greater than 15. The overall effect of the Rayleigh scattering on the angular distribution of the TOA reflectance is shown in Figure 2(b). The polar plot is normalized with the value in the nadir direction (shown in Figure 2(a)). In particular, Figure 2(b) shows that the anisotropy in the TOA reflectance in the presence of Rayleigh scattering is greater than the anisotropy of a cloud layer alone. The ratio of reflectances ($\rho^{atm}/\rho^{no\text{-}atm}$) is larger in the forward direction than in the backward direction. For example, in the principal plane at θ=60° in the forward direction (φ=0°), the value of the ratio is about 1.55, whereas at the same angle θ=60° in the backward direction (φ=180°), it is about 1.20. The effect of the Rayleigh scattering is weak in the plane that is perpendicular to the principal plane.

For these directions, the value of the ratio ($\rho^{atm}/\rho^{no\text{-}atm}$) is either 1 or slightly higher than 1 for most of the polar angles.

3.2 Altitude Dependence

Because the TOA reflectance increases from the Rayleigh scattering, particularly when the cloud optical thickness is small, one might expect that the reflectance should also change with cloud altitude. Figure 3 shows that this is not the case. For a given solar zenith angle, the ratio of the reflectances for two scenarios of cloud height, one with cloud top at 500 hPa and the other with cloud top at 700 hPa (ρ_{500}/ρ_{700}), hardly varies by more than 1%. At small values of solar zenith angle (θ_0), the ratio is slightly greater than 1, and at large values of θ_0, it is slightly less than 1. The reason for this difference is that for small values of θ_0, the contribution to the TOA reflectance, from the direct component of the solar irradiation falling on the cloud, is larger for cloud top at 500 hPa than for cloud top at 700 hPa. Furthermore, the larger contribution for cloud top at 500 hPa offsets any increased Rayleigh contribution from the atmosphere between 500 and 700 hPa. This finding explains why for small values of θ_0, the ratio of reflectances (ρ_{500}/ρ_{700}) in the nadir direction is greater than 1. On the other hand, at large values of θ_0, the contribution from the direct component, due to large slant path, is very small and ρ_{500}/ρ_{700} is primarily determined by the path radiance and the reflected downwelling diffused radiation falling on the cloud top. Because of increased atmospheric contribution for the cloud top at 700 hPa, ρ_{700} is greater than ρ_{500}, and as a result, the ratio (ρ_{500}/ρ_{700}) is greater than 1.

3.3 Surface Albedo Effects

The model results for 380-nm TOA nadir reflectance over low-reflecting surfaces (representing land and ocean) and high-reflecting surfaces (representing snow) are shown in Figures 4(a) and 4(b), respectively. These figures show that in most cases (τ_{cloud} >3), the nadir reflectance increases with an increase in τ_{cloud} but decreases with an increase in θ_0. The exceptions are for thin clouds, when $\tau_{cloud} < 3$. For example, one finds that for the small value of surface albedo (R_g=0.08) and $\theta_0 > 62^\circ$, the nadir reflectance increases with an increase in solar zenith angle (see Figure 3(a)). Also, for large values of surface albedo (for example, R_g=0.8) and $\tau_{cloud} < 3$, the nadir reflectance increases with τ_{cloud} for $\theta_0 \leq 30^\circ$ but decreases with τ_{cloud} for $\theta_0 > 62^\circ$. The increase in the nadir reflectance for $\theta_0 > 62^\circ$ in Figure 4(a) can be understood from the fact that at very large values of θ_0, the slant path through the thin cloud layer becomes large and that most of the scattering occurs near the top of the cloud. Increased scattering near the top of the cloud increases the upwelling radiation above the cloud, which results in increased reflectance at the TOA. The situation in Figure 4(b) can be understood in the following way: For small values of θ_0 and τ_{cloud} (< 3), most of the photons in the direct beam pass through the thin cloud and reach the high-reflecting ground. Similarly, most of the photons that are taken out of the direct beam in the thin cloud layer continue in the forward direction and reach the high-reflecting ground. At the ground, they are reflected back into the atmosphere, where they are multiply scattered in the molecular atmosphere as well as in the cloud layer and, finally, emerge at the TOA. For thin clouds, the scattering contribution from the cloud layer is larger than any attenuation caused by the cloud layer. This scattering contribution results in an increase in TOA reflectance for thin clouds at small values of

θ_0. However, for large values of θ_0, the attenuation through the thin cloud increases; therefore, a smaller number of photons reach the ground. As a result, the contribution of the high-reflecting ground to the TOA reflectance decreases, which causes the TOA reflectance to decrease with an increase in τ_{cloud}. After some τ_{cloud} value ($\tau_{cloud} > 3$), the contribution from multiple scattering in the cloud increases, and the TOA reflectance increases with the increase in the value of τ_{cloud}. This is true for all values of θ_0. It is interesting to note that at large solar zenith angles and bright surfaces, clouds can actually reduce the TOA reflectance below the cloud-free value. This reduced TOA reflectance makes it difficult to detect clouds when the surface is snow or ice covered.

3.4 Spectral Dependence

The model results for the ratio of the reflectances (ρ_{340}/ρ_{380}) for ground and ocean, and snow are shown in Figures 5(a) and 5(b), respectively. The most interesting feature in Figure 5(a) (low-reflecting surface) is that for a cloud-free atmosphere, the ratio, ρ_{340}/ρ_{380}, is about 1.3 for overhead sun and that it decreases with an increase in cloud optical thickness. The large value of the ratio, ρ_{340}/ρ_{380}, is primarily due to the Rayleigh scattering, where optical thickness is proportional to λ^{-4}. In other words, almost 60% difference in Rayleigh optical thickness between 340 nm and 380 nm results in ~30% difference in TOA reflectances. The inhibition of spectral contrast for the pure Rayleigh atmosphere is due to multiple scattering effects and the fact that the TOA albedo cannot exceed the value of unity. Clouds further inhibit spectral contrast of the TOA reflectance as seen in Figure 5(a). As the cloud optical thickness increases, the relative contribution in TOA reflectance from the cloud layer, which represents the scattering by large

particles, increases, and at large optical thickness (about τ_{cloud}=20), the ratio gets closer to 1. It is also interesting to note that for solar zenith angles less than 62°, the ratio very weakly depends on the solar zenith angle.

For high-reflecting ground with spectrally independent albedo (snow), we find that the spectral ratio, ρ_{340}/ρ_{380}, is close to unity even in the absence of clouds (Figure 5(b)). For overhead sun, the ratio is about 1.016 and decreases with an increase in solar zenith angle. However, as cloud optical thickness increases and becomes more than 3, the ratio becomes independent of the optical thickness of the cloud. For example, the ratio is about 0.995 for overhead sun and increases slightly to 1.035 for θ_0=78°. Also, it is interesting to note that for large values of θ_0, the value of the ratio, ρ_{340}/ρ_{380}, for all values of τ_{cloud} >0, is higher than its value for τ_{cloud}=0, the cloud-free, clear-sky value. This finding implies that one may detect cloud over snow (assuming that actual snow reflectance is close to Lambertian). The actual TOMS data show significant variation in ρ_{340}/ρ_{380} values over Antarctica, which could be explained by non-Lambertian snow reflectance (Warren et al., 1998) or cloud effects, or both. However, because of a lack of ground-based cloud data over the Antarctic continent, the observation noted above has not been positively correlated with clouds.

4.0 Comparison of Cloud Models With TOMS Data

The test for any model is that its predictions are in good agreement with measured data. In the preceding sections, we presented most of the Plane-Parallel Cloud (PPC) model results as a function of cloud optical thickness; however, cloud optical thickness is

not an observable quantity. The observable quantity is the scene reflectance, which, of course, is proportional to the cloud optical thickness (at least for thin clouds and low-ground albedo). Below, we present the results on the comparison of observed and computed reflectances to validate the PPC model. The results are presented in terms of ratios of reflectances, ρ_{340}/ρ_{380} versus ρ_{380}. Analyzing the data in this way has one advantage; that is, the wavelength dependence predicted by the model can be directly compared with the wavelength dependence observed in the data.

The results presented below are for low values of "ground" reflectivity. Because ocean reflectivity is generally small (~0.06), TOMS data over the oceans were selected to test the predictions of cloud models. Results for a number of solar zenith angles were examined; however, only results for 30° (±1°) and 62° (±1°) are presented here. TOMS 1986 data over the southern hemisphere oceans from equator to -60 degree latitude were used in the analysis. The data were screened for absorbing aerosols. (For these aerosols, the scene Lambert Equivalent Reflectivity (LER) at 340 nm is always less than the scene LER at 380 nm.) Also, only nadir observations were used to minimize the variability of the viewing-angle geometry. Finally, the 340-nm reflectances were corrected, in the first order, for column ozone amount in the atmosphere.

Figures 6(a) and 6(b), respectively, show the 340-nm to 380-nm reflectance ratio (ρ_{340}/ρ_{380}) as a function of ρ_{380} for the solar zenith angles of 30° and 62°. These figures also contain the results of the PPC model (discussed in Section 3), which are also discussed in the subsection below. The scatter diagrams in the figures show well-defined

parabolas with a very small amount of scatter around the mean curve. The small amount of scatter in the data is surprising, when one realizes that a typical TOMS pixel may contain a wide variety of clouds of differing sizes, shapes, thicknesses, and heights causing Mie scattering and Rayleigh scattering to interact in complicated ways. Qualitatively, one can explain the observed feature (the parabolic behavior) in the following way: At low-reflectance values, either the cloud optical thickness is very small or the clouds fill only a small portion of the 50- x 50-km TOMS pixel, so the ratio of reflectances is primarily determined by the Rayleigh scattering in the atmosphere. Therefore, 340-nm reflectance values will always be higher than the 380-nm reflectance values, and the ratio will always be greater than 1. As the cloud optical thickness increases, the contribution from the cloud scattering increases. Because the scattering contribution from the clouds is wavelength independent, the ratio of the reflectance values decreases with an increase in cloud optical thickness. As a result, at very large cloud optical thickness, the scene reflectance approaches its maximum value and the spectral ratio approaches unity, which are also seen in the data.

In the following subsections, we test the ability of three different cloud models to explain the spectral behavior observed in the TOMS data.

4.1 Comparison With the PPC Model

The solid lines in Figures 6(a) and 6(b) show the results from the PPC model that we have discussed in the previous sections. The model does a very good job of explaining the behavior of the observed data. However, it is not obvious why the agreement is so good, for the model contains only one parameter, the cloud optical

thickness. This parameter is determined from 380-nm top-of-the atmosphere (TOA) reflectance (Krotkov et al., 2001), with no other adjustable parameters. This finding suggests that in the case of the spectral dependence of TOA reflectance, clouds of various sizes and shapes can be approximated by an effective 100% cloud fraction and an effective optical thickness. The good agreement between the data and model persists over a large range of solar zenith angles, except for contamination from UV-absorbing aerosols, like smoke and mineral dust from the deserts, which occurs episodically. The effect of these aerosols on UV radiation is now well understood (Torres et al., 1998), and the perturbation they produce from the well-defined parabola of the type shown in Figures 6(a) and 6(b) is the basis of the TOMS-derived Aerosol Index (AI). The AI is now widely used for detecting UV-absorbing aerosols from satellite sensors (Herman et al., 1997). A unique feature of AI is that it can detect such aerosols even in the presence of clouds. This capability is possible only because the cloud-produced scatter in the TOA reflectance ratios is very small (see Figure 6).

4.2 Comparison With the LER Model

The LER model was first introduced by Mateer et al. (1971) to operationally process buv -type data from space. In this model, the cloud is treated as an opaque Lambertian-reflecting surface, and its reflectivity is obtained from the measured TOA reflectance from a non-ozone-absorbing channel of the instrument. Also, in this model, the cloud top pressure is determined from the LER value of the scene. For small values of LER (< 0.2), the cloud top pressure is generally taken as the terrain pressure, whereas for large values of LER (> 0.6), the cloud top pressure is set to the climatological cloud

top pressure. For LER values between 0.2 and 0.6, the cloud top pressure is the weighted mean of the terrain and the climatological cloud top pressure. The model also assumes that cloud top pressure determined in this manner is independent of wavelength. Figures 7(a) and 7(b) show a comparison of LER cloud model results with the TOMS data. We find that the LER model simply cannot explain the actual spectral dependence observed in the TOMS data. To make the model results agree with the data, one would have to place the clouds below the surface. This finding clearly suggests that the LER model should not be used to process buv-type data.

4.3 Comparison With the Mixed-LER (MLER) Model

The MLER model was introduced in the early 1990s to improve the agreement between the cloud model and the observed buv data. This model is also known as the Partial-Cloud model (McPeters et al., 1996; Hsu et al., 1997) or the Effective Cloud Fraction model [Koelemeijer and Stammes, 1999]. This model also treats clouds as opaque Lambertian reflectors, but with a caveat. It sets the cloud reflectivity at some large value to justify the assumption that clouds do not transmit any light from the atmosphere below. The radiance from this assumed surface is then mixed with clear-scene radiance, with the mixing fraction derived using the TOA reflectance at a particular wavelength. Figures 8(a) and 8(b) show that the MLER model agrees far better with the TOMS data than the LER model, provided one sets the cloud reflectivity at 0.8. Because most clouds are not very bright, the cloud fraction one derives using the MLER model is usually much smaller than the geometrical cloud fraction one derives from high-resolution visible instruments using the threshold technique (Rossow and Schiffer, 1999). Qualitatively, MLER gives a "radiative cloud fraction" in which radiation passing

through or around the cloud is treated similarly. However, in most implementations (McPeters et al., 1996) of MLER, the cloud reflectivity is held fixed at 0.8 regardless of solar zenith and viewing angles. But because the cloud BRDF (and TOA reflectance) varies with illumination and viewing angles, the cloud fraction of a given scene that one derives using the MLER model will also vary with the viewing angles. Stated differently, the cloud fraction derived using MLER from one viewing angle cannot be used to predict the TOA reflectance at another viewing angle. Despite these limitations, the MLER model is easy to implement and has provided reasonable estimates of cloud top pressure when applied to Global Ozone Mapping Experiment (GOME) data taken in the O_2-A absorption band near 760 nm (Koelemeijer et al., 2001) and in the O_2-O_2 absorption band near 480 nm (Acarreta and Haan, 2000).

5. Effect of Clouds on Tropospheric O_3 Absorption

Although the accuracy of the column ozone retrieved by buv-type satellite instruments is very high (~ ± 1%), the accuracy of the tropospheric column ozone (TCO) is highly problematic. This is the case for two reasons: First, very little ozone is in the troposphere (~10% of the total column), and second, the buv instruments are not very sensitive to the changes in the tropospheric ozone. With the awareness of the climatic changes due to human activities, accurate determination of the TCO has become very important. This is because the ozone in the troposphere is primarily produced by the photochemical reactions, particularly oxidation reactions involving NO_x, hydrocarbons, and CO. Indirect satellite residual methods (e.g., Fishman et al., 1990; Hudson and Thompson, 1998; Ziemke et al., 1998; Fishman and Balok, 1999; and Ziemke et al.,

2001) are currently used to estimate the TCO globally, and the accuracy depends on the assumptions and methodology used in the retrieval scheme. In this section, we address the effect of tropospheric ozone in the cloud layer on the TOA reflectance measured in the ozone-absorbing channels of the buv-type instruments. Here, we have selected TOMS' 317-nm channel for this purpose.

In the preceding sections, we have shown that the LER model does not accurately represent the scattering processes in the presence of clouds in the atmosphere. However, at very high TOA reflectance values, it correctly accounts for additional absorption due to multiple scattering between the cloud and the atmosphere above it, but it fails to account for any transmission of radiation in and through the clouds. Radiative transfer simulations show that photons do penetrate and get multiply scattered in the cloud layer, and after the scattering process, they re-emerge as reflected and transmitted photons. These findings can be better understood from the weighting function diagrams (Figure 9) for the following two cloud types: one, a mid-level cumulus cloud with top at 500 hPa, and the other, a convective cloud with top at 200 hPa. The weighting function simply represents the sensitivity of the TOA reflectance to the layer-ozone amount at different heights in the atmosphere.

The weighting functions in Figure 9 clearly show that for the mid-level cumulus cloud, the sensitivity to layer-ozone amount increases as one approaches the top of the cloud and that maximum sensitivity is closer to the top of the cloud. On the other hand, for the convective cloud, increased sensitivity begins near the top of the cloud surface,

and the peak is closer to 1/3 distance from the top of the cloud. The increased sensitivity above the cloud top for the mid-level cloud can be understood from the fact that 50% of the molecular atmosphere is above the cloud. As a result, more photons are multiply scattered between the cloud top and the atmosphere above, resulting in increased sensitivity above the cloud. For the convective cloud, only 20 percent of the molecular atmosphere is above the cloud top; hence, sensitivity to layer-ozone amount just above the cloud is small.

From the above discussion, it follows that in the presence of thick clouds, the LER-based ozone retrieval scheme would overestimate the column ozone amount in the atmosphere. The overestimation would depend on the location, geometric and optical thickness, and amount of ozone in the cloud layer.

These findings have an important bearing on the TCO reported in the literature. For example, we know that over the tropical Pacific Ocean, the TCO generally varies from 15 to 20 DU, whereas over the tropical Atlantic Ocean, the TCO varies from 35 to 40 DU. Therefore, TCO estimates that are based on the LER method for column ozone would have a larger error in the tropical Atlantic Ocean than over the Pacific Ocean. Estimates of the actual error would require error propagation through the TCO retrieval scheme, which is outside the scope of the current work.

6.0 Summary and Conclusions

In this paper, we showed that in the UV part of the spectrum, the Rayleigh scattering modifies the Bi-directional Reflectance Distribution Function (BRDF) properties of clouds. The ratio of the top of the atmosphere reflectance to the BRDF of the cloud (the reflectance in the absence of any atmosphere) is higher in the forward direction ($\varphi < 90^{o}$) than in the backward direction ($\varphi > 90^{o}$). We also found that for small values of cloud optical thickness, the Rayleigh scattering contribution from the molecular atmosphere is much larger than the Mie scattering contribution from the cloud. We further found that the ratio strongly depends on the solar zenith angle of the incident radiation. The ratio is about 3.5 for overhead sun and about 5.8 for a solar zenith angle of 78^{o}. However, with an increase in cloud optical thickness, the Mie scattering contribution from the cloud overwhelms the Rayleigh scattering from the molecular atmosphere. One finds that the ratio is practically 1 for cloud optical thickness greater than 15. In addition, for mid-level and low-level clouds, the ratio (at a given solar zenith angle) hardly varies by more than 1%.

The model results show that for a cloud-free atmosphere, the value of the ratio of the reflectances (ρ_{340}/ρ_{380}) - the spectral contrast varies from 1.31 to 1.34 for $\theta_o \leq 62^{o}$ and approaches unity at very large values of cloud optical thickness (τ_{cloud}). This result is because at small values of τ_{cloud}, Rayleigh scattering, which is proportional to λ^{-4}, contributes significantly to the reflectance values at both wavelengths. As the optical thickness increases, the contribution from the cloud layer, which represents the scattering

by large particles, increases resulting in the ratio to approach unity at very large values of τ_{cloud}.

We also compared the predictions of three cloud models: the Lambert Equivalent Reflectivity (LER) model, the Mixed-LER (MLER) model, and the Plane-Parallel Cloud (PPC) model with TOMS data over the oceans, where the surface reflectivity values are generally in the range of 5 to 8 %. The ratio of reflectances (ρ_{340}/ρ_{380}), which provides information on the wavelength dependence of the reflectances, was used to test the applicability of the models. With regard to the LER model, we found that in order to make the model results agree with the TOMS data, one would have to place the clouds below the true surface. This simply means that the LER model is not satisfactory to interpret buv data under cloudy conditions. The MLER model (also known as the Partial-Cloud model [McPeters et al., 1996; Hsu et al., 1997] or the Effective Cloud Fraction model [Koelemeijer and Stammes, 1999]) agrees fairly well with the TOMS data, provided one sets the reflectivity of the surface representing the cloud at 0.8. Because most clouds are not very bright, the cloud fraction that one derives using the MLER model is usually smaller than the cloud fraction one derives from high-resolution visible instruments using the threshold technique (Rossow et al., 1993). With regard to the PPC model, we found that the model accurately predicts the behavior of the observed data. This is remarkable considering that the model contains only one parameter, the cloud optical thickness, with no other adjustable parameters. This further suggests that in the case of the spectral dependence of the TOA reflectance , clouds of various sizes and shapes can be approximated by an effective optical thickness. The good agreement

between the data and the PPC model persists over a large range of solar zenith and viewing angles observed by TOMS, except for snow- or ice-covered pixels, or when the TOMS pixel contains large amounts of UV-absorbing aerosols (smoke and mineral dust from the deserts).

Finally, we examined the effect of clouds on the tropospheric column ozone (TCO) retrieval from the BUV technique. The TCO is generally retrieved using residual methods where one either subtracts the stratospheric column ozone (SCO) determined from the Stratospheric Aerosol and Gas Experiment (SAGE) or SBUV instruments or determines the ozone above the top of convective clouds assuming the LER model of the clouds. We examined the weighting function diagrams for two cloud types: one, a mid-level cumulus cloud with top at 500 hPa, and the other, a convective cloud with top at 200 hPa. The weighting function simply represents the sensitivity of the TOA reflectance to layer-ozone amount at different heights in the atmosphere. We found that for the mid-level cumulus cloud, the sensitivity to layer-ozone amount increases as one approaches the top of the cloud and that maximum sensitivity is closer to the top of the cloud. On the other hand, for the convective cloud, the increase in sensitivity begins near the top of the cloud surface and the peak is closer to 1/3 the distance from the top of the cloud. The results of the weighting functions imply that in the presence of thick clouds, the LER- or MLER-based ozone retrieval scheme would overestimate the column ozone amount in the atmosphere. This overestimation would occur because these models do not account for transfer of radiation in and through the cloud. Also, the overestimation would depend on the location and amount of ozone in the cloud layer. For example, TCO estimates

would have a larger error in the tropical Atlantic Ocean than over the Pacific Ocean. This is because the surface measurements of the TCO over the Atlantic Ocean are about 35 to 40 DU, whereas the measurements over the Pacific Ocean indicate the TCO is about 15 to 20 DU. Estimates of the actual error would require error propagation through the TCO retrieval algorithm, which is outside the scope of the current work.

7.0 References

Acarreta, J. R. and J. F. de Haan, Cloud pressure algorithm based on O_2-O_2 absorption, in OMI algorithm theoretical basis document, volume 3 Clouds, aerosols and surface UV irradiance, edited by P. Stammes and R. Noordhoek, EOS/AURA online document, 2002

Ahmad, Z. and R. S. Fraser, An iterative radiative transfer code for ocean-atmosphere system, J. Atmos. Sci., 39, 656-665, 1982.

Bhartia, P.K., R. D. McPeters, C. L. Mateer, L. E. Flynn, and C. Wellemeyer, Algorithm for the estimation of vertical profiles from the backscattered ultraviolet technique, *J. Geophys. Res.* 101, 18793-18806, 1996.

Burrows, J. P., M. Weber, M. Buchwitz, V. V. Rozanov, A. Ladstaetter-Weisenmeyer, A.Richter, R. de Beek, R.Hoogen, Bramstadt, K.-U. Eichmann, M. Eisinger, and D. Perner, The Global Ozone Monitoring Experiment (GOME): mission concept and first scientific results, *J. Atmos. Sci.*, 56, 151-175, 1999.

Chance, K. Analysis of BrO measurements from the Global Ozone Monitoring Experiment, *Geophys. Res. Lett.*, 25, 3335-3338, 1998.

Chance, K., P. I. Palmer, R. Spurr, R. V. Martin, T. P. Kurosu, and D. J. Jacob, Satellite observations of formaldehyde over North America from GOME, *Geophys. Res. Lett.*, 27, 3461-3464, 2000.

Deirmendjian, D., ICES Electromagnetic Scattering, M. Kerker (ed.) Pergamon Press, Oxford, 592 pp., 1963

Deirmendjian, D., Appl. Optics, 3, 187-196, 1964.

Deirmendjian, D., Electromagnetic scattering on spherical polydispersions, Elsevier, 290, 1969.

Fishman, J., C. E. Watson, J. C. Larson, and J. A. Logan, Distribution of tropospheric ozone determined from satellite data. *J. Geophys. Res.*, 105, 3599-3617, 1990.

Fishman, J., and A. E. Balok, Calculation of daily tropospheric ozone residuals using TOMS and empirically improved SBUV measurements: Application to an ozone pollution episode over the eastern United States, *J. Geophys. Res.*, 104, 30,319-30,340, 1999.

Fraser, R.S., and Z. Ahmad, The effect of surface reflection and clouds on the estimation of total ozone from satellite measurements, Fourth NASA Weather and Climate Program

Science Review, *NASA Conf. Publ. 2076,* 247-252, National Aeronautics and Space Administration, Washington, D.C., [NTIS N790633],1978.

Hansen, J.E., Multiple scattering of polarized light in planetary atmosphere. Part I. The doubling method, J. Atmos. Sci., 36, 508,518, 1971(1976?).

Herman, B.M., and S.R. Browning, 1965, A numerical solution to the equation of radiative transfer, *J. Atmos. Sci.*, 22, 559-566, 1965.

Herman, J.R, P.K. Bhartia, A.J. Krueger, R D. McPeters, C.G. Wellemeyer, G. Jaross, B.M. Schlesinger, O. Torres, G. Lobow, W. Byerly, S.L. Taylor, T. Swissler, R.P. Cebula, and X-Y Gu, Meteor-3 Total Ozone Mapping Spectrometer (TOMS) Data Products User's Guide, *NASA Ref. Publ.*, 1996.

Herman, J.R. , P.K. Bhartia, O. Torres, C. Hsu, C.Seftor, and E. Celarier, "Global distibution of UV-absorbing aerosols from Nimbus-7/TOMS data", *J.Geophys. Res.*, 102, 16911- (1997).

Hsu , N.C., R.D.McPeters, C. J. Seftor, and A.M.Thompson, Effect of an improved cloud climatology on the total ozone mapping spectrometer total ozone retrieval, J. Geophys. Res., 102, 4247-4255, 1997

Hudson, R. D., and A. M. Thompson, Tropical tropospheric ozone (TTO) from TOMS by a modified-residual method. *J. Geophys. Res.*, 101, 24,069-24,082, 1996.

Klenk, K.F., P.K. Bhartia, A.J. Fleig, V.G. Kaveeshwar, R.D. McPeters, and P.M. Smith, Total ozone determination from Backscattered Ultraviolet (BUV) experiment, *J. Appl. Meteor.*, 21, 1672-1684, 1982.

King, M.D., and Harshvardhan, Comparative accuracy of the albedo, transmission and absorption for selected radiative approximation, NASA Reference Publication 1160, 1986.

King, M.D., Determination of the scaled optical thickness of clouds from reflected solar radiation measurements, *J. Atmos. Sci.*, 44, 1734-1751, 1987.

Koelemeijer , R.B.A. and P. Stammes, Effects of clouds on ozone column retrieval from GOME UV measurements, J. Geophys. Res.., 104, 8281-8294, 1999

Koelemeijer , R.B.A. and P. Stammes, Comparison of cloud retrievals from GOME and ATSR-2, *Earth Obs. Quart.*, 65, 25-27, 2000

Koelemeijer , R.B.A. , P. Stammes, J.W. Hovenier, and J.F. de Haan, A fast method for retrieval of cloud parameters using oxygen A-band measurements from GOME, *J. Geophys. Res.* , 106, 3475-3490, 2001

Figure Captions

Figure 1(a) The nadir reflectance of clouds in the absence of molecular atmosphere as functions of solar zenith angle (θ_0) and optical thickness (τ_{cloud}). The results are for a ground reflectivity (R_g) of 0.

Figure 1(b) The Bi-directional Reflectance Distribution Function (BRDF) of a cloud layer at 380 nm. The BRDF values are normalized with respect to the value in the nadir direction. The results are for cloud optical thickness (τ_{cloud}) of 10, the solar zenith angle (θ_0) of 62°, and the ground reflectivity (R_g) of 0.

Figure 2(a) The ratio of top-of-the atmosphere (TOA) nadir reflectance with atmosphere to the nadir reflectance without atmosphere ($\rho^{atm}/\rho^{no\text{-}atm}$) as functions of cloud optical thickness (τ_{cloud}) and solar zenith angle (θ_0). Here, the wavelength is 380 nm and the ground reflectivity (R_g) is 0.

Figure 2(b) The angular dependence of the ratio ($\rho^{atm}/\rho^{no\text{-}atm}$) for a solar zenith angle of 62° and cloud optical thickness of 10. The reflectance values are normalized with the value in the nadir direction.

Figure 3 The ratio of the top-of-the atmosphere (TOA) reflectances at 380- nm wavelength for two cloud top pressures: 500 and 700 hPa. The ground reflectivity (R_g) is 0.

Figure 4(a) The top-of-the atmosphere (TOA) nadir reflectance of clouds in the presence of molecular atmosphere as functions of solar zenith angle (θ_0) and optical thickness (τ_{cloud}). Here, the ground reflectivity (R_g) is 0.08.

Figure 4(b) Same as in Figure 4(a) but for a high-reflecting surface (R_g=0.80).

Figure 5(a) The ratio of nadir TOA reflectances (TOARs) over a low-reflecting surface (R_g=0.08) as functions of solar zenith angle (θ_0) and optical thickness (τ_{cloud}).

Figure 5(b) Same as in Figure 5(a) but for a high-reflecting surface (R_g=0.80)

Figure 6(a) Scatter diagram of the TOMS-measured ratio of 340- and 380-nm reflectances to 380-nm reflectance. Only TOMS nadir samples over the southern hemisphere oceans are used in the scatter diagram. The solid line is a result of the Plane-Parallel Cloud (PPC) model. The results presented here are for a solar zenith angle of 30° (±1°).

Figure 6(b) Same as in Figure 6(a) but for a solar zenith angle of 62° (±1°).

Figure 7(a) Same as in Figure 6(a) except the model results are obtained using the LER model in which clouds are assumed to be opaque Lambertian reflectors. The solid and dashed lines are derived assuming the surface is located at 1.0 and 0.5 atm, respectively.

Figure 7(b) Same as in Figure 7(a) but for a solar zenith angle of 62° (±1°).

Figs 8(a) Same as in Figure 6(a) except the lines are obtained from the MLER model in which radiances from Lambertian surfaces of reflectivity 0.6, 0.7, 0.8, 0.9, and 1.0, representing clouds, are linearly mixed with radiance from another surface at reflectivity 0.08, representing the true surface.

Figure 8(b) Same as in Figure 8(a) but for a solar zenith angle of 62° (±1°).

Figure 9 The weighting functions for the 317-nm channel of the TOMS instrument in the presence of a convective cloud (solid line) and a cumulus cloud (dashed line). The cloud top for the convective cloud is at 200 hPa (11 km) and the bottom is at 800 hPa (1.8 km). For the mid-level cumulus cloud, the cloud top is at 500 hPa (5.6 km) and the bottom is at 700 hPa (3.0 km). The geometric thickness for the two cloud layers is 9.2 and 2.6 km. The dotted star line represents the weighting function for a cloud-free molecular atmosphere. All weighting functions are to their stratospheric values at 25 km.

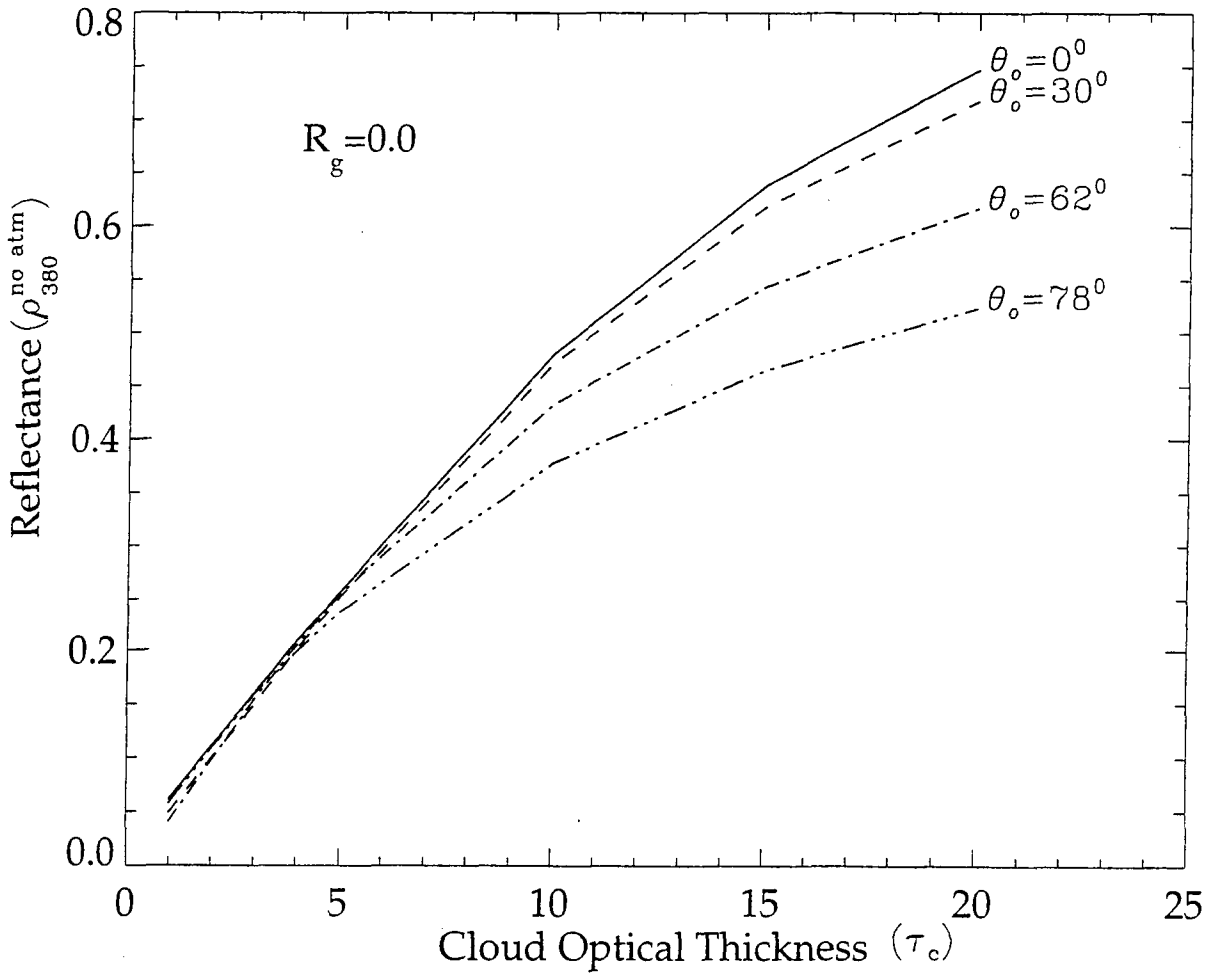

Fig 1(a)

/misc/ahmad/RADTRAN/utfnl_figs/cld0.proFig_1

BRDF of the cloud:tau_cld=10,SZA=62,and Rg=0.0
BRDF is normalized wrt reflectance in the nadir direction

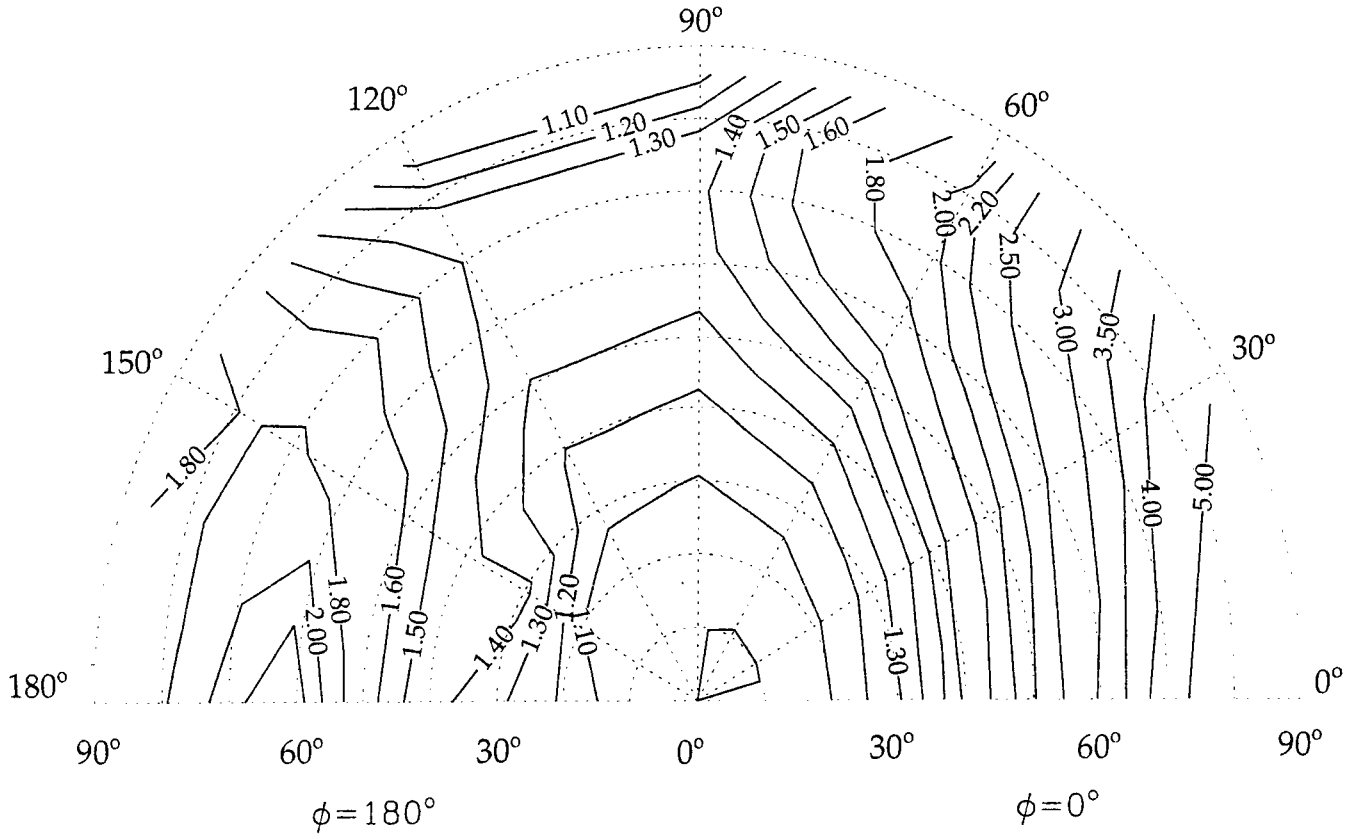

Fig 1(b)

/misc/ahmad/RADTRAN/utfnl_figs/brdf380.proFig_2

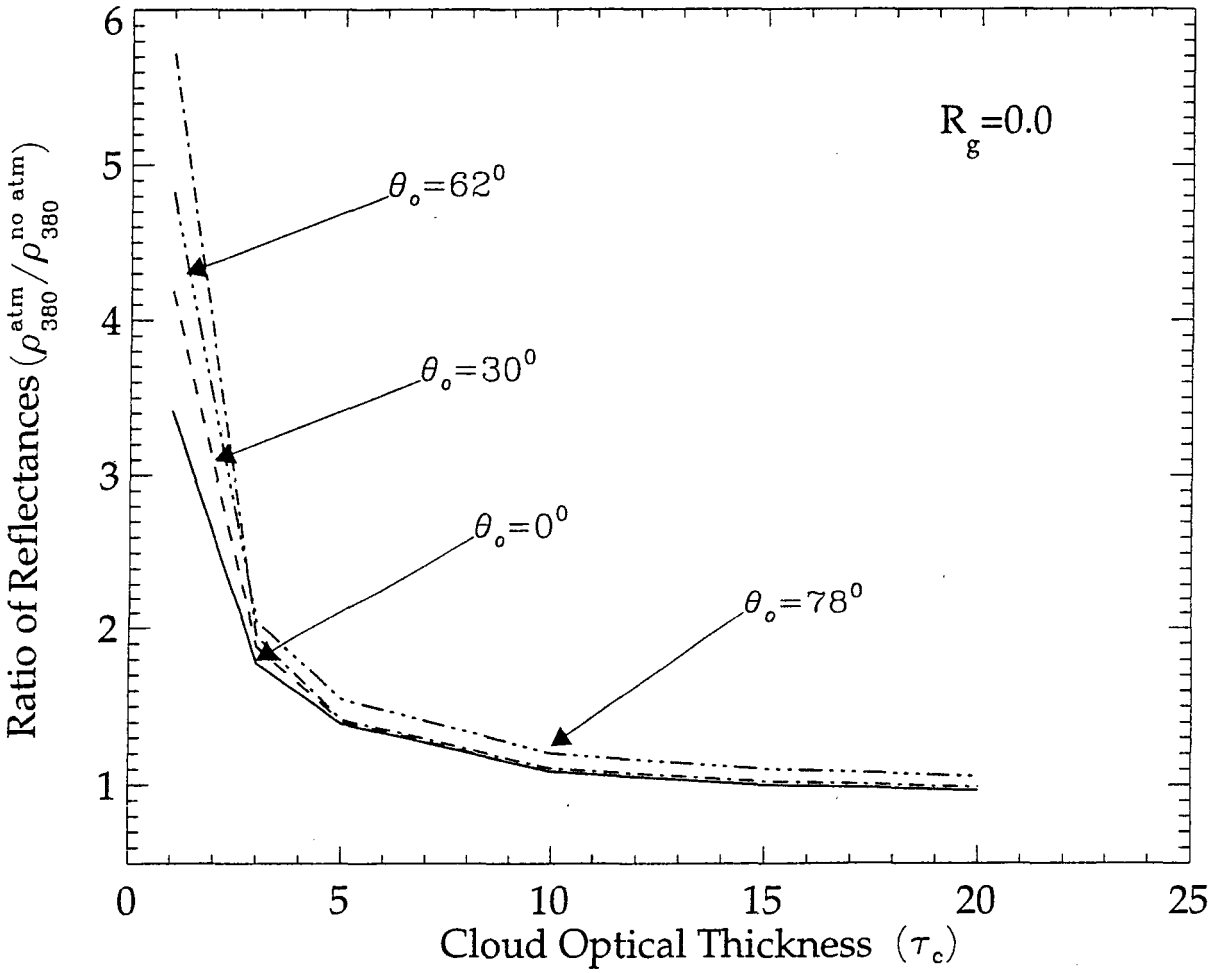

Fig 2(a)

/misc/ahmad/RADTRAN/utfnl_figs/cld0.proFig_3

iRatio of Top of the Atm. Reflectance to BRDF of the cloud:tau_cld=10,SZA=62,and Rg=0.0
The ratio of TOA Reflectance to BRDF is normalized wrt reflectance in the nadir direction

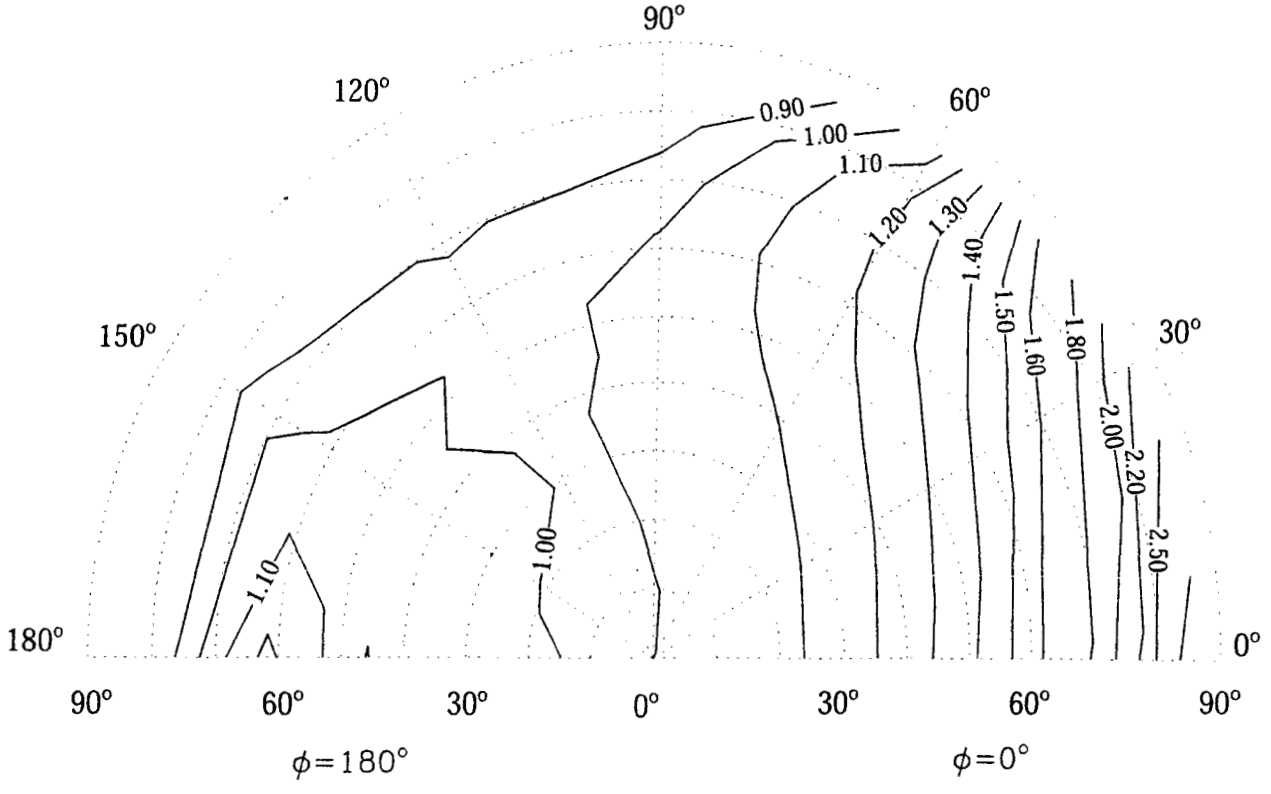

/misc/ahmad/RADTRAN/utfnl_figs/brdf380.proFig_2A

Fig 2(b)

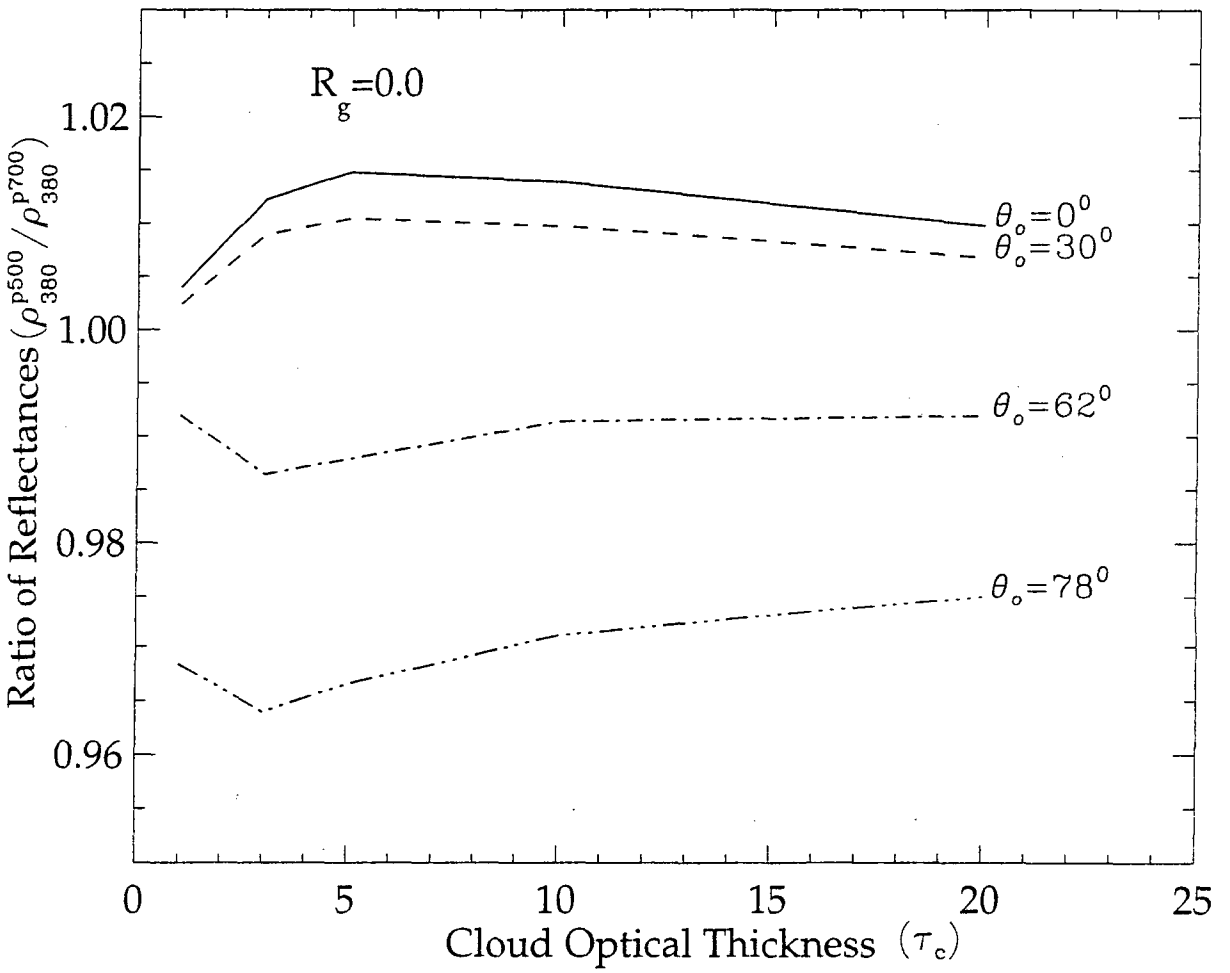

/misc/ahmad/RADTRAN/utfnl_figs/cld_Fig4.pro

Fig 3

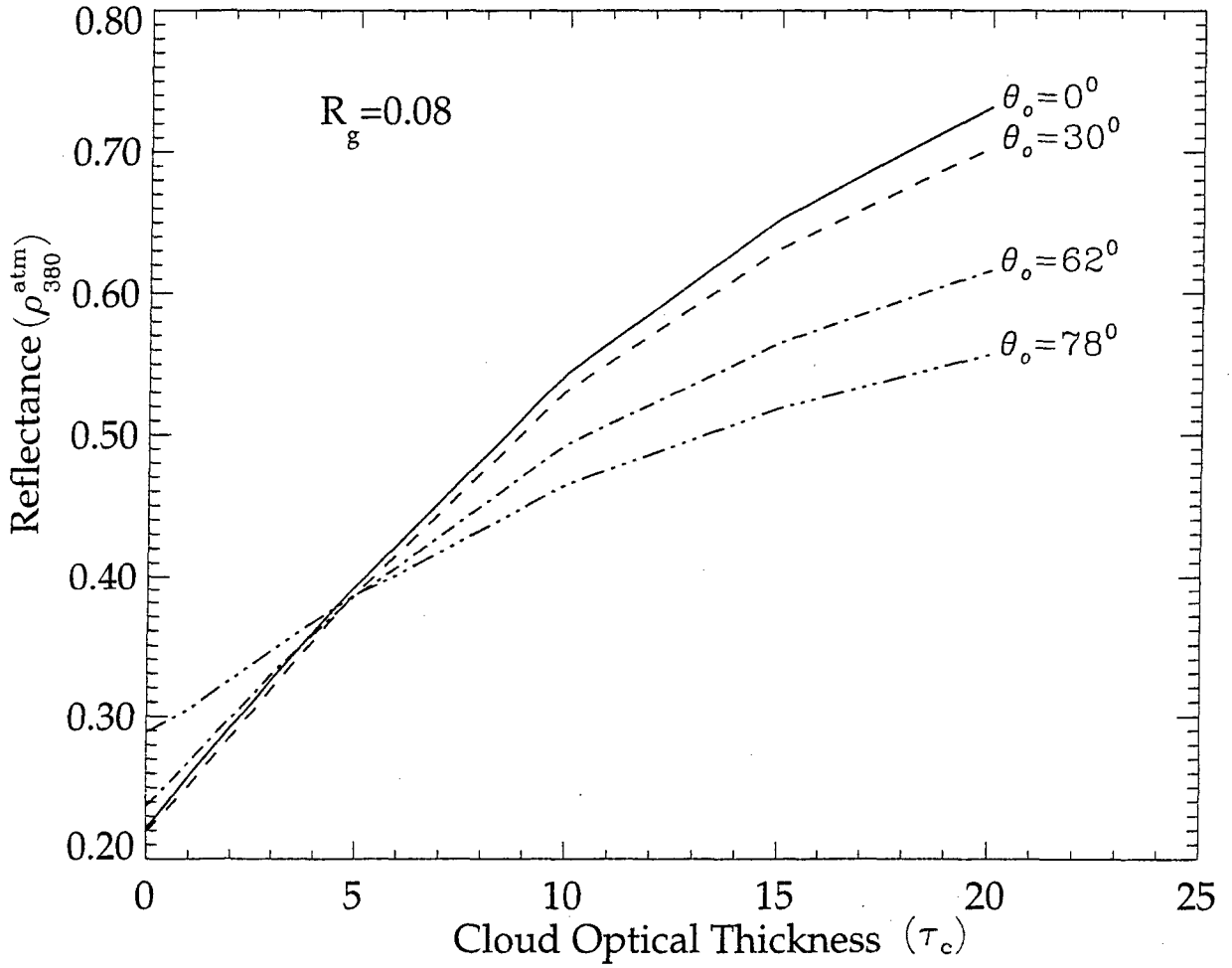

/misc/ahmad/RADTRAN/utfnl_figs/cld_Fig5.proFig_5a

Fig 4(a)

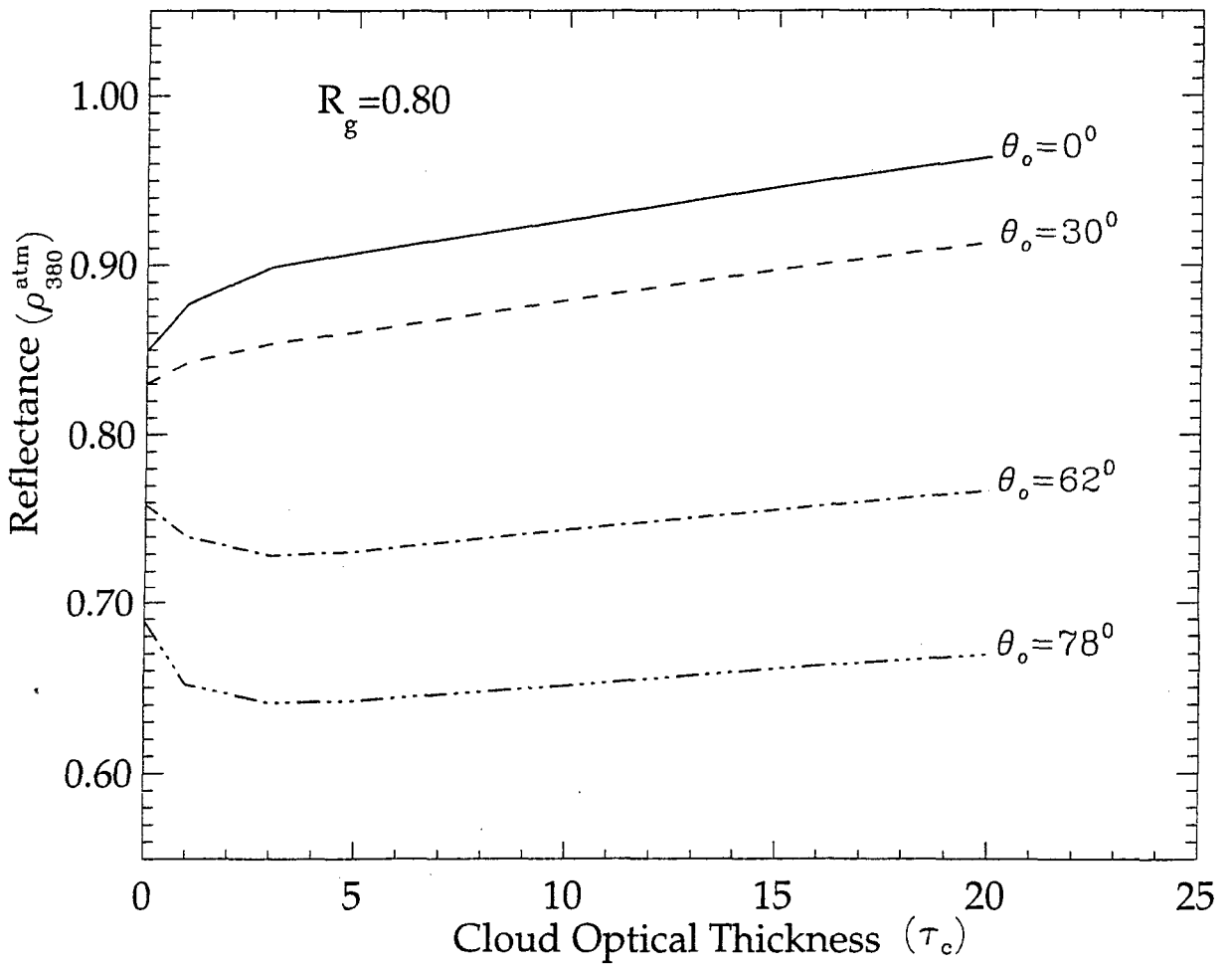

/misc/ahmad/RADTRAN/utfnl_figs/cld_Fig5.proFig_5b

Fig 4(b)

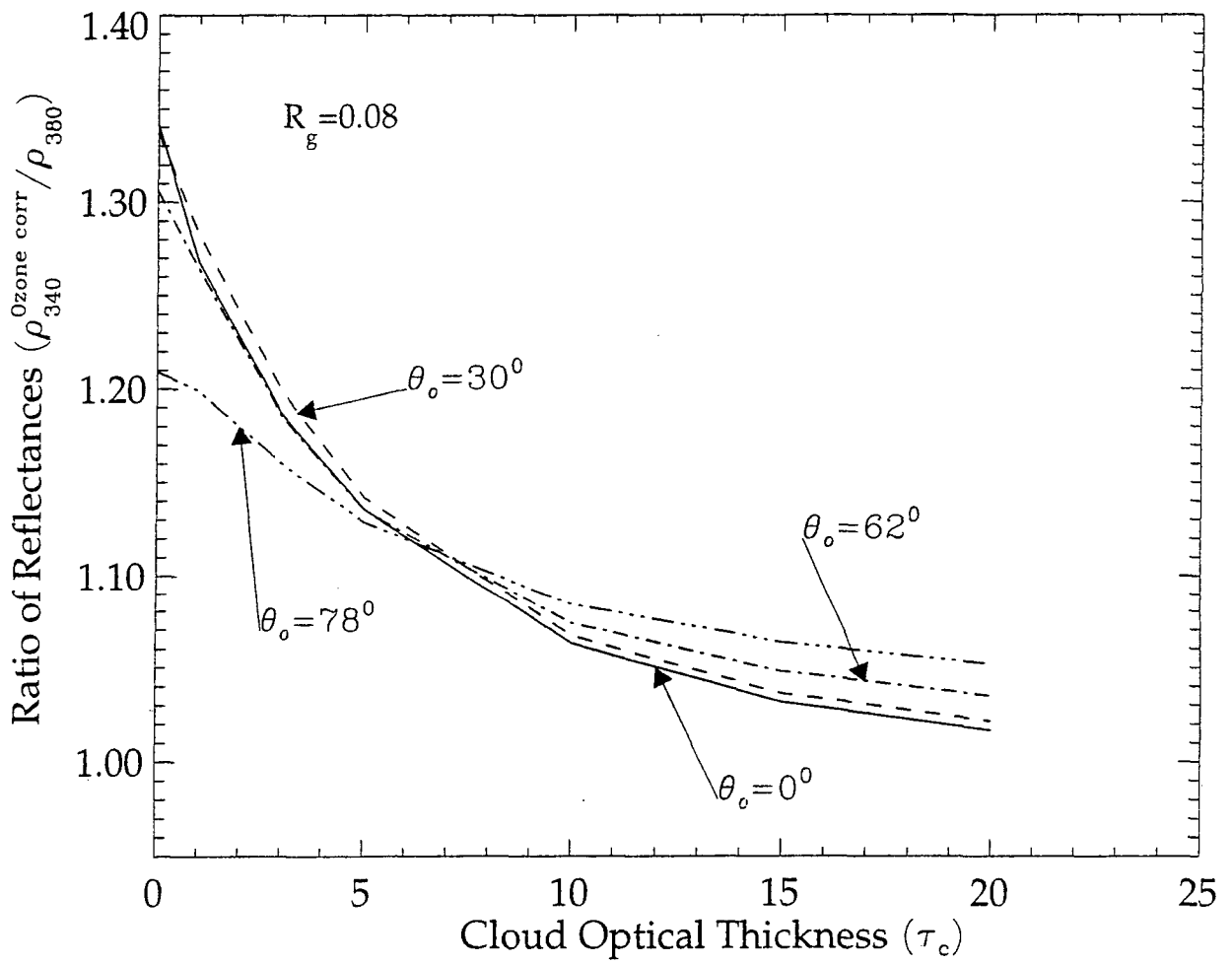

Fig 5(a)

/misc/ahmad/RADTRAN/utfnl_figs/fig6.pro

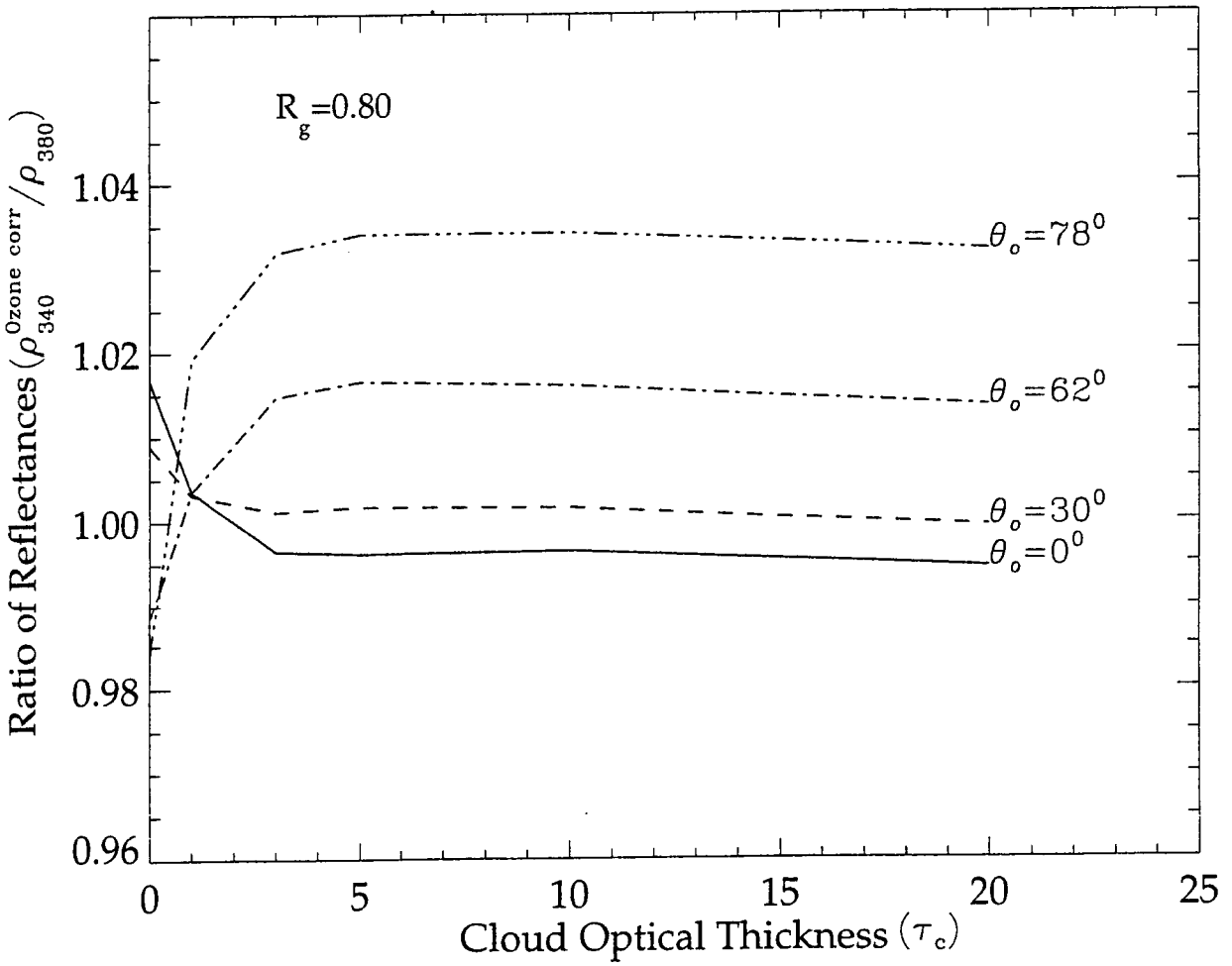

Fig 5(b)

/misc/ahmad/RADTRAN/utfnl_figs/fig6.pro

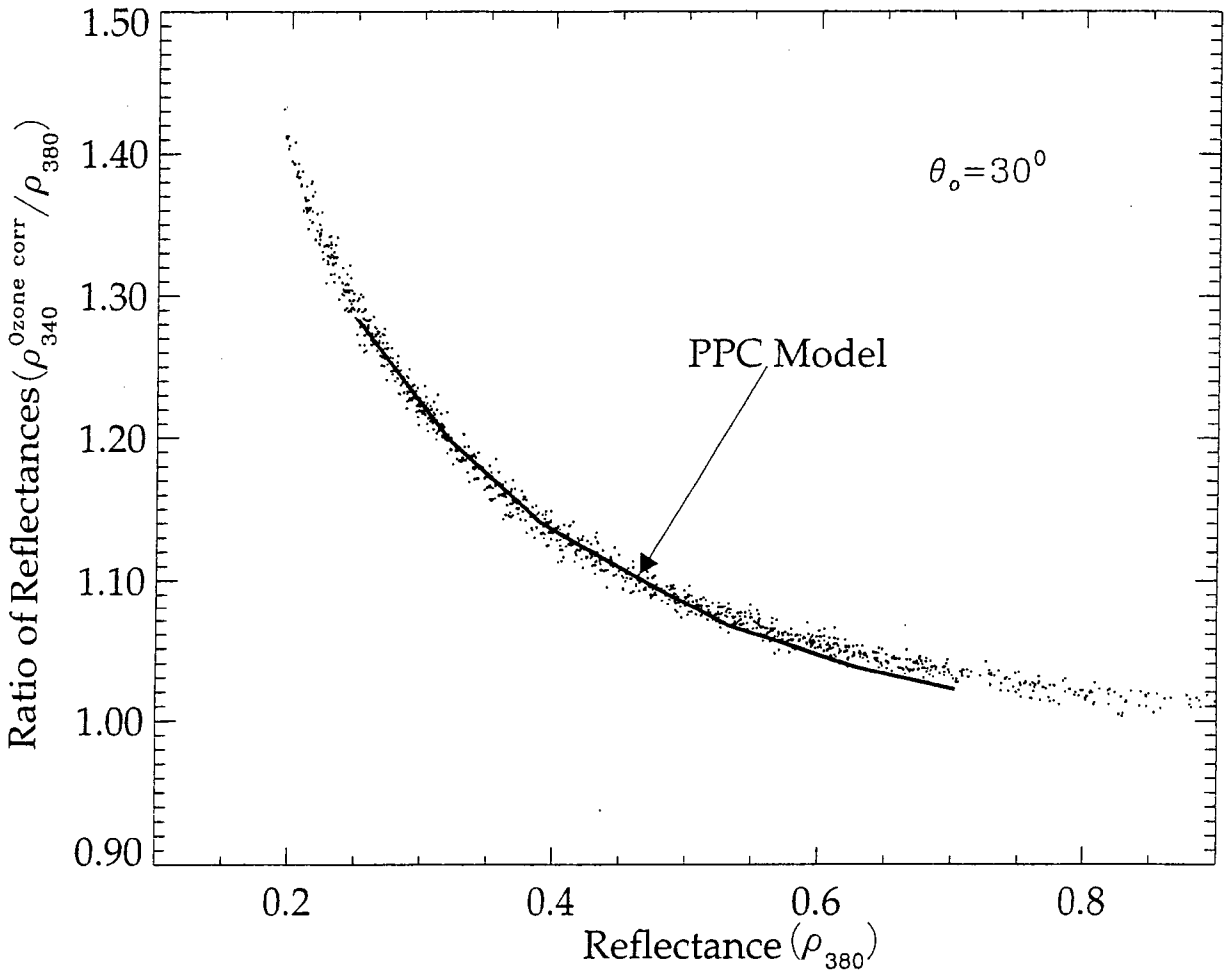

Fig 6(a)

/misc/ahmad/RADTRAN/utfnl_figsII/fig7a.pro

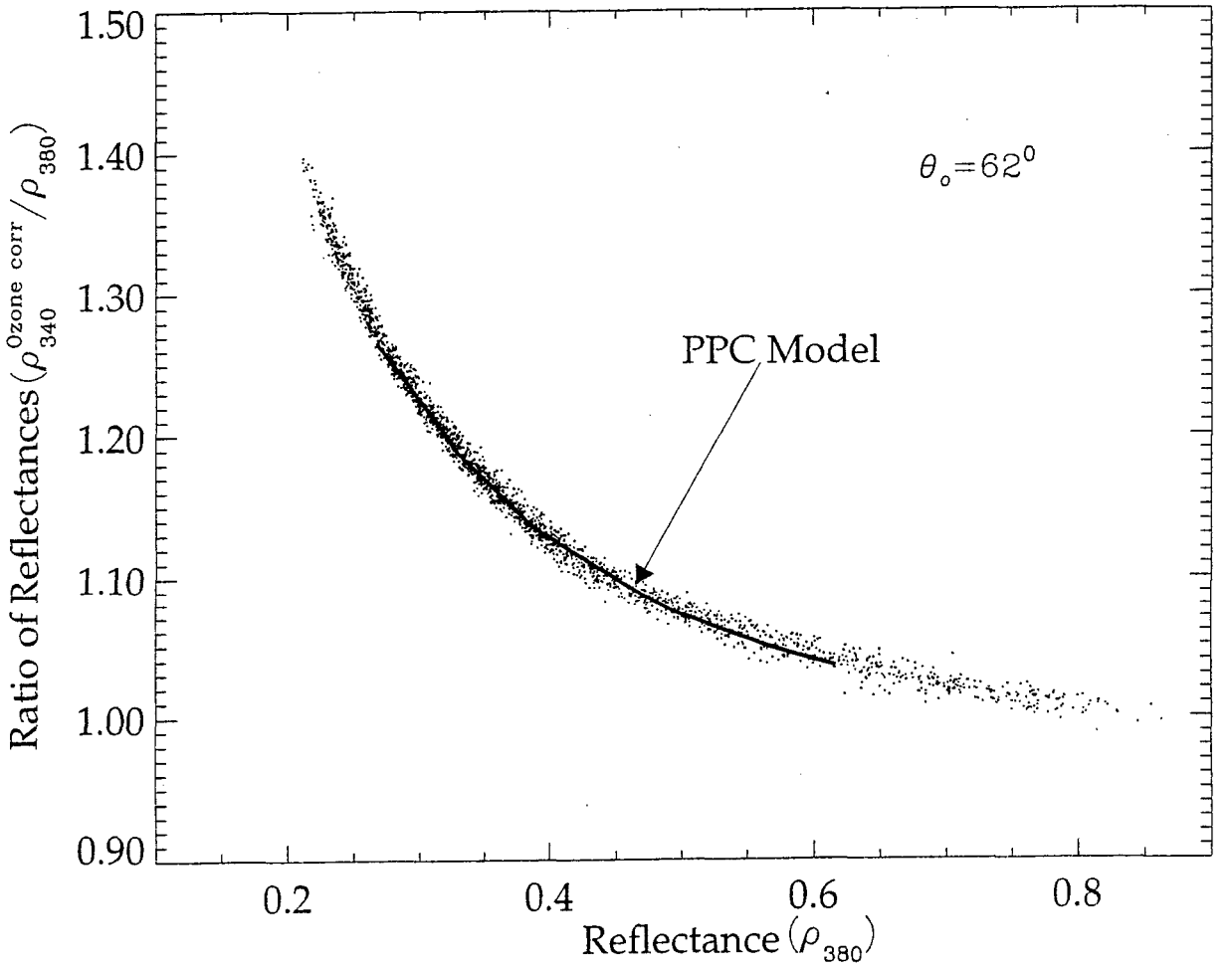

Fig 6(b)

/misc/ahmad/RADTRAN/utfnl_figsII/fig7a.pro

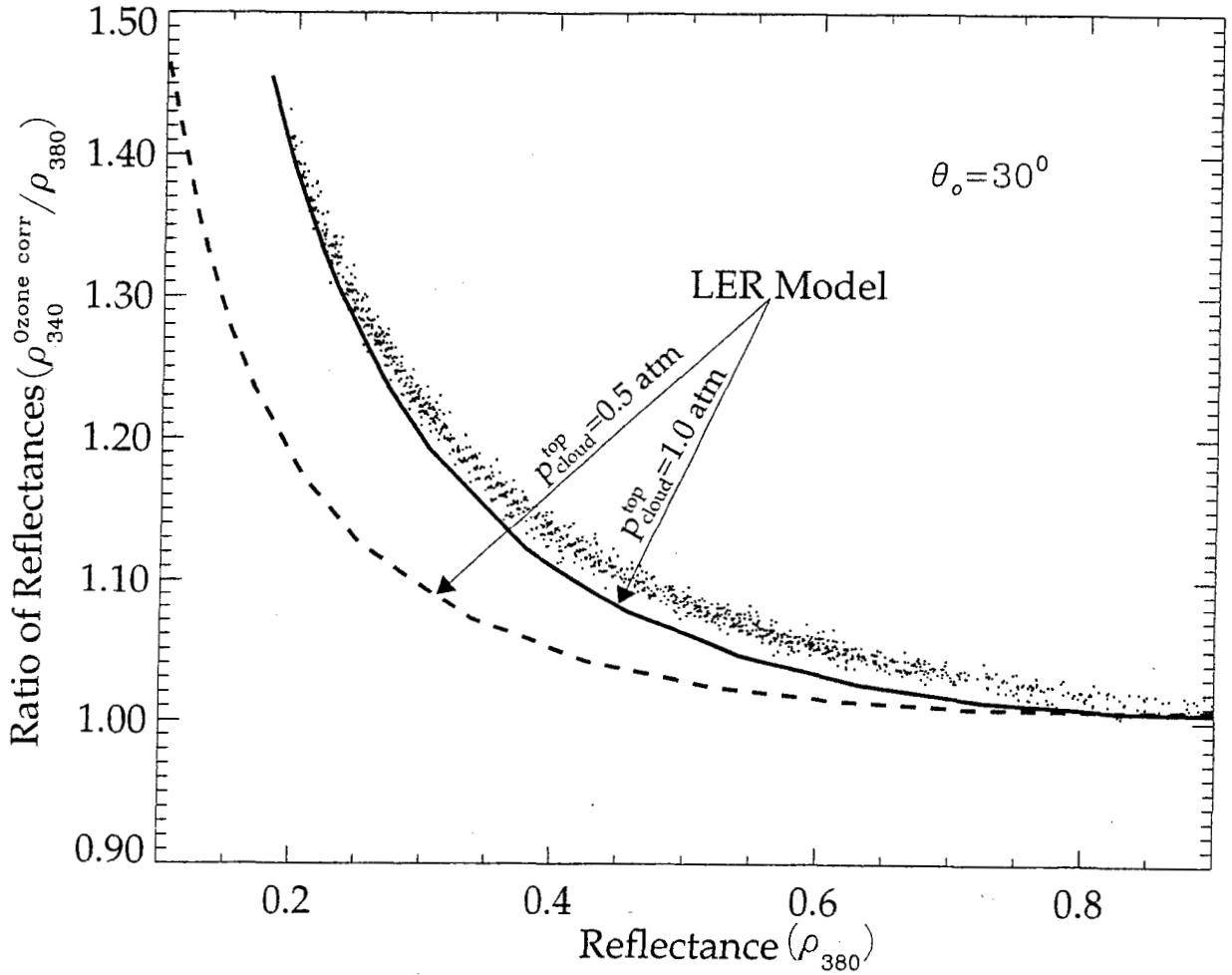

Fig 7(a)

/misc/ahmad/RADTRAN/utfnl_figsII/fig8a.pro

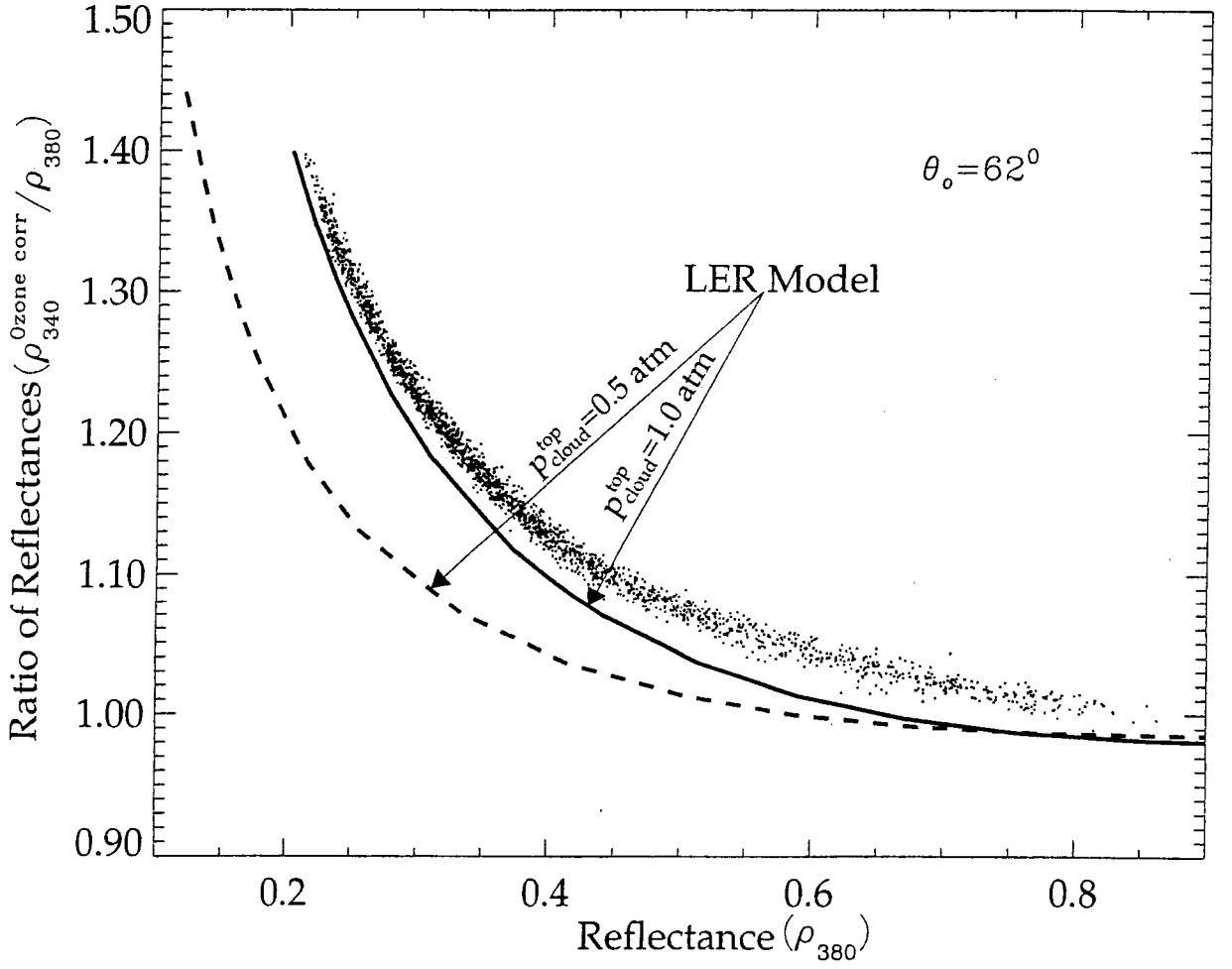

Fig 7(b)

/misc/ahmad/RADTRAN/utfnl_figsII/fig8a.pro

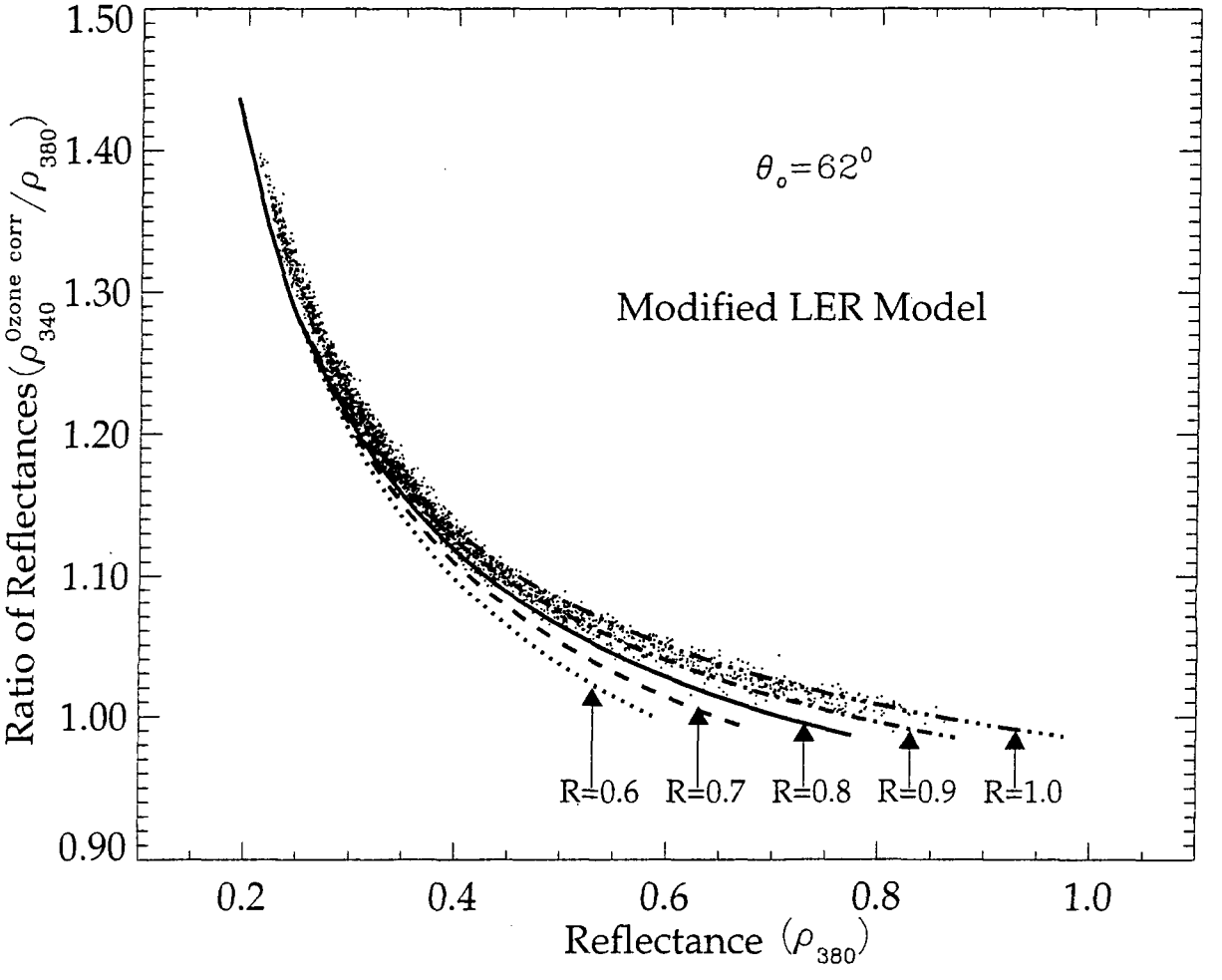

Fig 8(a)

/misc/ahmad/RADTRAN/utfnl_figsII/fig9a.pro

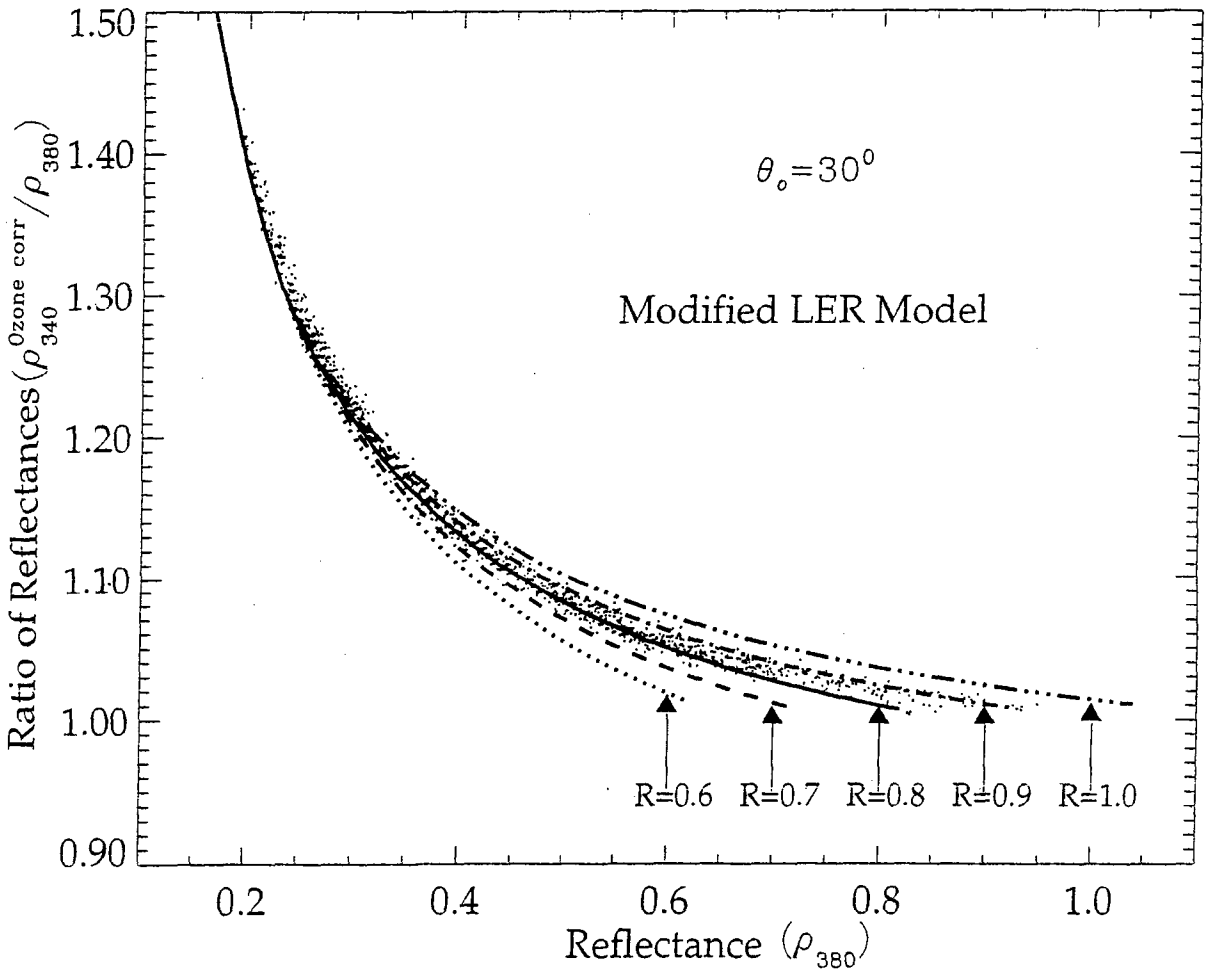

Fig 8(b)

/misc/ahmad/RADTRAN/utfnl_figsII/fig9a.pro

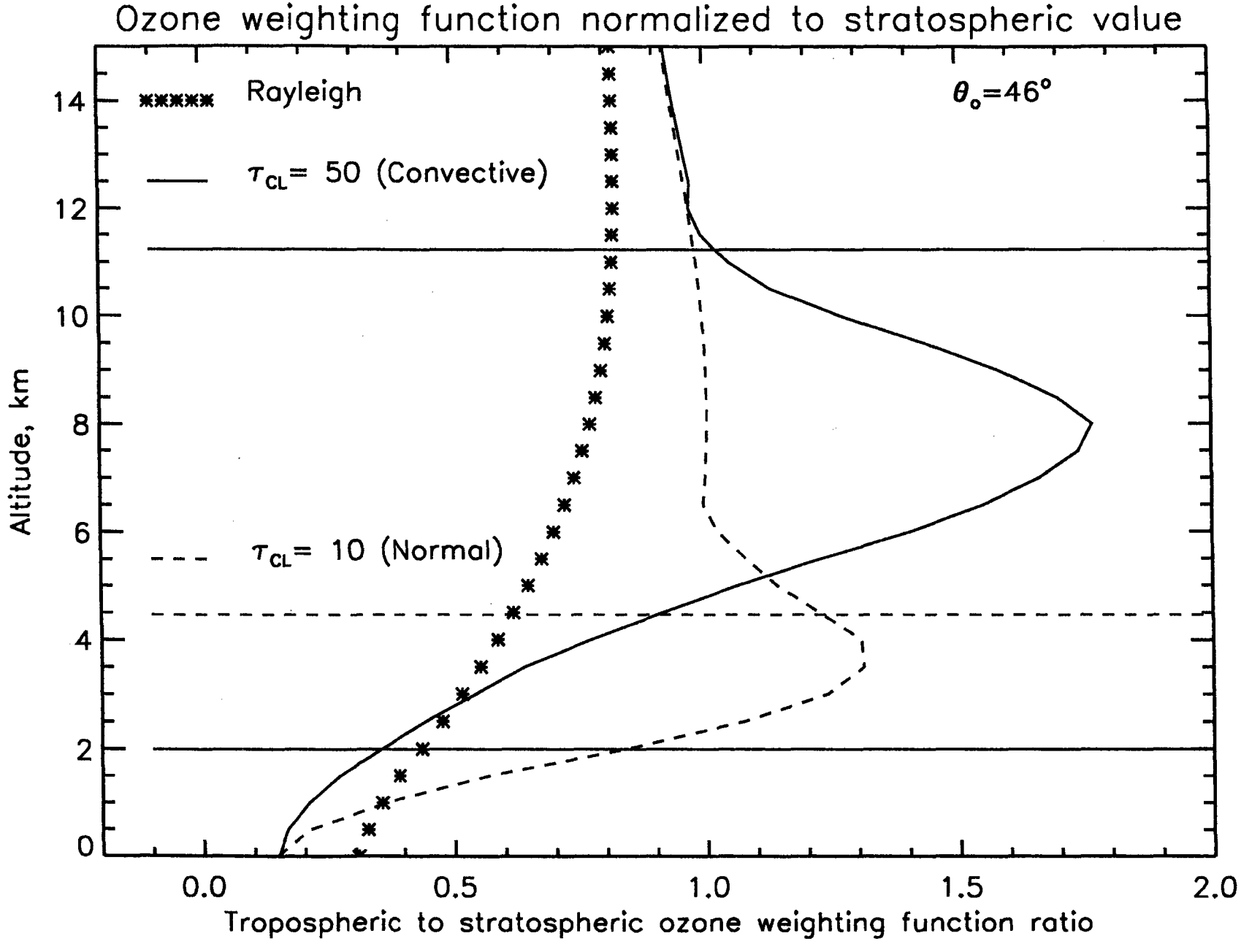
Ozone weighting function normalized to stratospheric value
Rayleigh
θ_o=46°
τ_{CL}= 50 (Convective)
τ_{CL}= 10 (Normal)
Altitude, km
0
2
4
6
8
10
12
14
0.0
0.5
1.0
1.5
2.0
Tropospheric to stratospheric ozone weighting function ratio

Fig 9